HHS Public Access

Author manuscript

J Autoimmun. Author manuscript; available in PMC 2018 November 20.

Published in final edited form as:

J Autoimmun. 2015 August ; 62: 81–92. doi:10.1016/j.jaut.2015.06.003.

Deletion of WASp and N-WASp in B cells cripples the germinal center response and results in production of IgM autoantibodies

Carin I.M. Dahlberg[a], **Magda-Liz Torres**[a], **Sven H. Petersen**[a], **Marisa A.P. Baptista**[a], **Marton Keszei**[a], **Stefano Volpi**[b], **Emilie K. Grasset**[a], **Mikael C.I. Karlsson**[a], **Jolan E. Walter**[b,c], **Scott B. Snapper**[d], **Luigi D. Notarangelo**[b], and **Lisa S. Westerberg**[a,*]

[a]Department of Microbiology Tumor and Cell Biology, Karolinska Institutet, Stockholm 171 77, Sweden

[b]Division of Immunology, Boston Children's Hospital, Harvard Medical School, Boston, MA 02115, USA

[c]Pediatric Immunodeficiency Program, Division of Allergy, Massachusetts General Hospital for Children, Boston, MA 02114, USA

[d]Gastroenterology Division, Children's Hospital, Harvard Medical School, Boston, MA 02115, USA

Abstract

Humoral immunodeficiency caused by mutations in the Wiskott-Aldrich syndrome protein (WASp) is associated with failure to respond to common pathogens and high frequency of autoimmunity. Here we addressed the question how deficiency in WASp and the homologous protein N-WASp skews the immune response towards autoreactivity. Mice devoid of WASp or both WASp and N-WASp in B cells formed germinal center to increased load of apoptotic cells as a source of autoantigens. However, the germinal centers showed abolished polarity and B cells retained longer and proliferated less in the germinal centers. While WASp-deficient mice had high titers of autoreactive IgG, B cells devoid of both WASp and N-WASp produced mainly IgM autoantibodies with broad reactivity to autoantigens. Moreover, B cells lacking both WASp and N-WASp induced somatic hypermutation at reduced frequency. Despite this, IgG1-expressing B cells devoid of WASp and N-WASp acquired a specific high affinity mutation, implying an increased BCR signaling threshold for selection in germinal centers. Our data provides evidence for that N-WASp expression alone drives WASp-deficient B cells towards autoimmunity.

Keywords

B cells; Germinal center; Autoimmunity; Primary immunodeficiency; Wiskott-Aldrich syndrome; N-WASp

*Corresponding author. Lisa.Westerberg@ki.se (L.S. Westerberg).

Conflict of interest

The authors declare no competing financial interests.

Appendix A. Supplementary data

Supplementary data related to this article can be found at http://dx.doi.org/10.1016/j.jaut.2015.06.003.

1. Introduction

Humoral immunity generates long-lived plasma cells and memory cells and depends on B cell affinity maturation in germinal centers (GCs). The GC is organized into two spatially separated zones. The light zone (LZ) of the GC contains the network of follicular dendritic cells (FDCs) that endocytose and recycle antigen to facilitate B cell affinity maturation [1]. The dark zone (DZ) consists of highly proliferating B cells that express activation induced deaminase (AID) to induce somatic hypermutation (SHM) and immunoglobulin (Ig) class switch recombination [2]. Newly mutated and Ig class switched B cells migrate from the DZ to test their BCR for antigen recognition in the LZ on antigen-covered FDCs and compete for help from antigen-specific T follicular helper (T_{FH}) cells [3,4]. The affinity of the B cell receptor (BCR) for the antigen on FDCs is proportional to antigen uptake and frequency of MHC class II – peptide presentation to T_{FH} cells [5]. Therefore, B cells that express BCR with high affinity for antigen out-competes B cells with low affinity BCR and only high affinity B cells develop into plasma cells and memory cells [4,5]. B cell migration between the DZ and LZ is mediated by the chemokine receptors CXCR4 and CXCR5 [6] and both interzonal migration [3] and intrazonal migration [7] drives SHM in the DZ and selection of B cells in the LZ.

Extensive cell migration, cell-to-cell communication, and cell division during the GC response critically rely on BCR signaling and the dynamics of the actin cytoskeleton. Signaling from the BCR to the actin cytoskeleton is regulated by the intracellular signaling axis of guanine exchange factors (GEFs, including Vav1, Vav2, and Dock8), that activate Rho GTPases (such as Cdc42, Rac1, and Rac2), that in turn activate WASp family members (such as WASp and N-WASp) [8,9]. While WASp is exclusively expressed in hematopoietic cells [10,11], the homologous protein N-WASp is ubiquitously expressed [12] and complete deletion of N-WASp is embryonic lethal [13]. Deletion of both WASp and N-WASp specifically in B or T cells markedly reduces B and T cell development and activation, implying that N-WASp can partially compensate for WASp deficiency [14,15]. Up to 70% of WAS patients develop autoimmune disease [16–18] and this has been attributed to defective suppression by $WASp^{-/-}$ T regulatory cells [19–22] and to intrinsic B cell dysfunction [23–25]. Moreover, three recent papers describe decreased BCR repertoire diversity in WAS patients associated with high production of autoantibodies [26–28]. Deletion of both WASp and N-WASp in B cells leads to absence of marginal zone (MZ) B cells associated with abolished IgG antibody responses to T-cell independent antigen [14]. Liu et al. recently showed that B cell specific deletion of N-WASp enhances and prolongs BCR signaling, suggesting that N-WASp is a critical negative regulator of B cell activation [29]. The exact function of WASp and N-WASp in the GC response and in regulation of peripheral B cell tolerance remains largely unknown.

Here we sought to define the role of WASp and N-WASp in the GC response to autoantigens and non-self antigen. To accomplish this, we used mice lacking WASp ($WASp^{-/-}$ mice) and mice lacking WASp and N-WASp in B cells ($WASp^{-/-}$N-$WASp^{fl/fl}CD19^{Cre/+}$ mice). We show that $WASp^{-/-}$ and $WASp^{-/-}$N-$WASp^{fl/fl}CD19^{Cre/+}$ mice formed GCs in response to apoptotic cells as a source of autoantigens, however, the GCs had reduced polarization into DZ and LZ and B cell retained longer and proliferated less in GCs. $WASp^{-/-}$ mice had

elevated titers of autoreactive IgG antibodies and generated high affinity IgG antibodies. In contrast, $WASp^{-/-}$N-$WASp^{fl/fl}CD19^{Cre/+}$ produced mainly IgM autoantibodies with broad reactivity to autoantigens and failed to induce increased titers of high affinity IgG antibodies. Our results suggest that N-WASp expression alone drives WASp-deficient B cells towards autoimmunity.

2. Material and methods

2.1. Mice and BM transfer

Mice were housed at the animal facility of the Department of Microbiology, Tumor and Cell Biology, Karolinska Institutet under specific pathogen-free conditions. Animal experiments were carried out after approval and in accordance with guidelines from the local ethical committee (North Stockholm district court). Wildtype, $WASp^{-/-}$, and $WASp^{-/-}$N-$WASp^{fl/fl}CD19^{Cre/+}$ mice were littermates from mixed allele breedings of WT 129Sv mice, $WASp^{-/-}$ mice on a 129Sv background, N-$WASp^{fl/fl}$ mice on 129Sv background, and $CD19^{Cre/+}$ mice on C57Bl/6 background. For generation of mixed bone marrow (BM) chimeras, 2×10^7 total BM cells containing $WASp^{-/-}$ or $WASp^{-/-}$N-$WASp^{fl/fl}CD19^{Cre/+}$ BM (expressing CD45.2) with wildtype BM (expressing CD45.1) at a 3:1 ratio were transplanted via intravenous injection into lethally irradiated (13 Gy) wildtype 129Sv recipient animals.

2.2. Apoptotic cell immunization and anti-DNA ELISA

The apoptotic cells were prepared from syngeneic thymocytes cultured for 6 h in complete RPMI 1640 and 1 μmM dexamethasone (Sigma–Aldrich). Age- and sex-matched littermate mice were injected intravenously weekly for 4 weeks with 10^7 apoptotic. Serum samples were collected weekly from the tail artery and anti-DNA autoantibodies were measured by ELISA [30,31]. In brief, anti-DNA titers of IgM and IgG were measured by ELISA using methylated BSA plus calf thymus DNA (Sigma–Aldrich) or total histone solution (Sigma–Aldrich) as capture. AP-conjugated secondary anti-IgM and -IgG antibodies (SouthernBiotech) were used for detection. As standard for analysis of serum from mice immunized with apoptotic cells, serial dilutions of a pool of serums from all samples was used. As standard for analysis of serum from 8 to 10 months old unchallenged mice, serial dilutions of an ANA positve B6.MRL-lpr or NZM2410 serum pool was used, or serial dilutions of mouse anti-human nucleosome IgG (BDbiosciences). All samples were tested in duplicates and corrected for background binding. Titration curves for IgM are shown in Supplementary Figure S1.

2.3. Labeling of apoptotic cells, immunohistochemistry and measurement in picture

Apoptotic cells were labeled with CFSE (Invitrogen) and analyzed by immunohistochemistry [32]. The following reagents were used: anti- B220 (RA3-6B2), -IgG1 (RMG1-1, BioLegend); -CD169 (MOMA-1; AbCam); -CD11c (HL3), -IgM (II/41), -CD35 (8C12; BD Biosciences), biotinylated peanut agglutinin (Vector Laboratories); goat anti-rat-AlexaFluor488, Strepavidin-Alexa-Fluor555 (Invitrogen). Images were collected with a Leica DM IRBE confocal laser scanning microscope (Leica Microsystems) equipped with 1 argon and 2 HeNe lasers, using an HC PL APO lens at 10x/0.40 CS and 90% glycerol

(MP Biomedicals) and processed with Adobe Photoshop CS5 (Adobe Systems). The areas of GCs (PNA^+), of follicular ($B220^+$ cells surrounded by $CD169^+$ cells) and areas of $CD35^+$ in GCs and $B220^+$ area (excluding MZ) were measured on three images from each mouse of random sections using Fiji, ImageJ software (National Institutes of Health), and the ratio was calculated.

2.4. Autoantibody arrays

Serum from naïve mice and mice immunized with apoptotic cells were screened for reactivity to 95 different autoantigens using autoantibody array (University of Texas Southwestern Medical Center, Genomic and Microarray Core Facility) [33]. The array was probed with serum samples, developed with Cy3-labeled anti-IgG and Cy5-labeled anti-IgM, and then scanned at 635 nm and 570 nm fluorescence, respectively. Data were visualized by using MultiExperimentViewer, Cluster 3.0 (Open Source software available at http://mev-tm4.sourceforge.net).

2.5. DC isolation and flow cytometry

For DC isolation, spleens were cut up into small fragments and incubated at 37 °C for 1 h in 1 mg/ml collagenase III (Worthington) and 120 μg/ml DNAse (Roche) in RPMI-1640 medium. For flow cytometry, data was acquired on a FACSFortessa flow cytometer (BD Biosciences) and analyzed using FlowJo Version 10 software for PC (TreeStar). The following antibodies were used: anti-$V_L1\lambda$ (R26-46), -CD62L (Mel14), -IgG1, -CD8 (53–6.7), -CD11b (M1/70), -CXCR4 (2BII/CXCR4), -CD44 (IM7), -CXCR5 (2G8), -GL7 (GL7), -CD95 (Jo2) (all BD Biosciences), -CD44 (eBioscience), Strepavidin-AlexaFluor555, LIVE/DEAD® (Invitrogen), -DEC205 (NLDC-145, Dendritics), -PD1 (RMP1-;30), -CD3 (145-2C11), -CD4 (RM4-5), -CD11c (N418), -CD83 (Michel-19), -33D1 (33D1), -B220 (RA3-6B2), -CD138 (281–2), -IgM (RMM-1) Streptavidin-APC-Cy7 (all Bio-Legend), -NP8, -NP24 (all Biosearch Technologies) and -IgG1 (SouthernBiotech).

2.6. EdU and BrdU incorporation

For continuous in vivo labeling of cells, mice were fed 5-ethynyl-2′-deoxyuridine (EdU, at 0.2 mg/mL) or bromodeoxyuridine (BrdU, at 0.3 mg/mL, Sigma–Aldrich, St Louis, MO) in the drinking water supplemented with 10% sucrose. EdU and BrdU incorporation in spleen cells was determined using the Click-iT® EdU cell proliferation assay (Invitrogen) and FITC BrdU flow kit (BD Biosciences).

2.7. T-B cell co-culture assay

WT, $WASp^{-/-}$ or $WASp^{-/-}$N-$WASp^{fl/fl}CD19^{Cre/+}$ splenic B cells were activated with anti-CD40 + IL-4 for 2 days. Cells were harvested, and incubated with affinity purified biotinylated F(ab')2 goat anti-mouse IgM (25 ng/ml; Jackson ImmunoResearch). B cells were then incubated with ovalbumin antigen delivery reagent (Miltenyi Biotec) diluted at 1:10. For synapse formation analysis B cells and $CD4^+$ OT-II T cells (1:5 ratio) were co-cultured for 2 h and then mounted on fibronectin (Invitrogen) coated slides and stained with B220 (RA3-6B2) (BioLegend) and phalloidin (Invitrogen). For the T cell proliferation assay, B cells and $CD4^+$ OT-II T cells (2:1 ratio) were co-cultured for 3 days. Four hours before

harvest, Phorbol myristate acetate (PMA, 0.5 μg/ml, Sigma–Aldrich), Ionomycin (0.5 ng/ml, Sigma–Aldrich) and GolgiPlug (1.4 μl/ml, BD Biosciences) were added. Cells were stained with anti-CD4 (eBioScience), B220, and lL-2 (BioLegend) and analyzed by FACSFortessa.

2.8. NP-KLH immunization, quantitative RT-PCR, spectratyping, and SHM analysis

Mice were immunized with 100 μg 4-Hydroxy-3-nitrophenylacetyl keyhole limpet hemocyanin (NP-KLH, Biosearch Technologies) in alum followed by a booster immunization with 100 μg NP-KLH in PBS at day 21. At day 28, mice were analyzed for serum NP-specific antibodies, VH gene usage by quantitative RT-PCR, spectratyping, and SHM. For *ELISA*, plates (Nunc) were coated with NP(4)-BSA or NP(26)-BSA (BiosearchTechnologies), serum added and analyzed for anti-NP IgM and IgG1 antibodies. The samples were run in duplicates and corrected for background binding. GC B cells were enriched by positive selection with biotinylated peanut agglutinin (Vector Laboratories), total RNA extracted using Trizol (Invitrogen), reverse transcriptase reaction performed using iScript-cDNA Synthesis Kit (Bio-Rad). *Quantitative RT-PCR* was conducted as previously [34,35] using degenerative V_H-specific forward primers and a common reverse primer in the J_H4 region; 5′-TTACCTGAGGAGACGGTGA-3′. Forward primers: (V_H1) MIGHV1, 5′-TCCAGCACAGCCTACATGCAGCTC-3′; (V_H2) M1GHV2, 5′-CAGGTGCAGCTGAAGGAGTCAGG-3′; and (V_H5) MIGHV5, 5′;-CAGCTGGTGGAGTCTGGGGGA-3′. Samples were run on a Bio-Rad CXF96 cycler and analyzed with the CFX Manager Software (Bio-Rad). For *spectratyping analysis* the same set of primers were used and the length of the CDR3 region of V_H1, V_H2, and V_H5 analyzed using Peak Scanner v1.0 software (Applied Biosystems). Gaussian distribution analyses on spectratyping data were calculated with non-linear regression analysis. For *SHM* analysis, $V_H186.2$ transcripts were amplified from cDNA of GC enriched B cells using a nested PCR approach. Primer sequences used in the first PCR: common forward primer $V_H186.2$ 5′ –GCTGTATCATGCTCTTCTTG-3′, reverse primer Cμ 5′-AGGGGGCTCTCGCAGGAGACGAGG-3′ or reverse primer Cε1 5′-GGATGACTCATCCCAGGGTCACCATGGAGT-3′. The second nested PCR primer sequences were: common forward primer $V_H186.2$ 5′-GGTGTCCACTCCCAGGTCCA-3′, reverse primer Cμ 5′-AGGGGGAAGACATTTGGGAAGGAC-3′ or Cε1 5′-CCAGGGGCCAGTGGATAGAC-3′. PCR products were cloned into TOPO TA (Invitrogen) and sequenced (Operon). Only unique sequences were analyzed for replacement mutations as determined by the ImMunoGeneTics (IMGT) database [36].

2.9. Statistical analysis

All experiments were analyzed by using Prism version 6.0 (GraphPad). All data were analyzed by ROUT (Q = 1.0%) in Prism version 6.0 and outliers excluded as indicated in figure legends. For statistics, a two-tailed unpaired Student's *t* test was used. A *P*-value <0.05 was considered statistically significant.

3. Results

3.1. WASp$^{-/-}$N-WASp$^{fl/fl}$CD19$^{Cre/+}$ mice have increased serum titers of DNA-specific IgM antibodies

To investigate the role of WASp and N-WASp in autoimmunity, we evoked an autoimmune response in WASp$^{-/-}$ and WASp$^{-/-}$N-WASp$^{fl/fl}$CD19$^{Cre/+}$ mice by immunization of autologous apoptotic thymocytes. Wildtype, WASp$^{-/-}$ and WASp$^{-/-}$N-WASp$^{fl/fl}$CD19$^{Cre/+}$ mice showed similar localization of injected fluorescently-labeled apoptotic cells to the MZ at 30 min after injection (Fig. 1A). We examined the distribution of CD11c^{+} DCs that transport apoptotic cells from the MZ into the B cell follicle [37]. In wildtype mice, CD11c^{+} cells mice localized preferentially in the T-B cell border (Fig. 1B). In contrast, CD11c^{+} cells covered the MZ and the Tcell area in WASp$^{-/-}$ and WASp$^{-/-}$N-WASp$^{fl/fl}$CD19$^{Cre/+}$ mice. In spleen cell analysis by flow cytometry, WASp$^{-/-}$ and WASp$^{-/-}$N-WASp$^{fl/fl}$CD19$^{Cre/+}$ mice had increased number of total CD11c^{+} cells, as well as of CD11c^{+}DEC205^{+} DCs and CD11c^{+}33D1^{+} DCs when compared to wildtype cells (Fig. 1C). To assess DC binding capacity to apoptotic cells, we examined co-localization of DCs with apoptotic cells 30 min upon injection of fluorescently-labeled apoptotic cells *in vivo*. Despite the increased number of CD11c^{+} DC subsets in WASp$^{-/-}$ and WASp$^{-/-}$N-WASp$^{fl/fl}$CD19$^{Cre/+}$ mice, similar number of CD11c^{+}DEC205^{+} DCs in wildtype, WASp$^{-/-}$, and WASp$^{-/-}$N-WASp$^{fl/fl}$CD19$^{Cre/+}$ mice bound apoptotic cells *in vivo* (Fig. 1D). We next examined the autoantibody response to apoptotic cells (Fig. 1E). In wildtype mice, self-tolerance was broken after two injections of apoptotic cells as measured by increased titers of IgG antibodies against DNA (Fig. 1G) [30,38]. As compared to wildtype and WASp$^{-/-}$ mice, WASp$^{-/-}$N-WASp$^{fl/fl}$CD19$^{Cre/+}$ mice had already before immunization increased titers of DNA-specific IgM that remained high after immunization with apoptotic cells (Fig. 1F). In the IgG response, WASp$^{-/-}$ mice had elevated titers of anti-DNA IgG antibodies already before immunization (Fig. 1G). At day 27 upon immunization with apoptotic cells, WASp$^{-/-}$ and WASp$^{-/-}$N-WASp$^{fl/fl}$CD19$^{Cre/+}$ mice had an IgG response towards DNA similar to wildtype mice (Fig. 1G).

3.2. WASp$^{-/-}$N-WASp$^{fl/fl}$CD19$^{Cre/+}$ mice have IgM autoantibodies to a broad range of autoantigens

Apoptotic cells are particulate antigens that harbor many selfepitopes besides DNA. To analyze the diversity of autoantibody production in WASp$^{-/-}$ and WASp$^{-/-}$N-WASp$^{fl/fl}$CD19$^{Cre/+}$ mice, serum from mice before and after immunization with apoptotic cells were screened for 95 autoantigens with the use of an autoantibody array. Wildtype mice induced an autoantibody response mainly consisting of IgG autoantibodies in response to apoptotic cells (Fig. 2A and B). WASp$^{-/-}$ mice had increased titers of autoreactive IgM and IgG antibodies before immunization as previously shown (Fig. 2A and B) [19,24]. Upon apoptotic cell immunization, WASp$^{-/-}$ mice showed an autoantibody response consisting of both IgM and IgG subtypes and of broad reactivity (Fig. 2A and B). WASp$^{-/-}$N-WASp$^{fl/fl}$CD19$^{Cre/+}$ mice showed high titers of IgM autoantibodies with diverse reactivity already before immunization with apoptotic cells, and upon immunization the IgM autoantibodies remained high and of broad reactivity (Fig. 2A). In response to apoptotic cells, IgG autoantibodies in WASp$^{-/-}$N-WASp$^{fl/fl}$CD19$^{Cre/+}$ mice had similar reactivity to

that of wildtype and WASp$^{-/-}$ mice (Fig. 2A and B). To examine if increased titers of DNA-specific IgM in WASp$^{-/-}$N-WASp$^{fl/fl}$CD19$^{Cre/+}$ mice would switch to pathogenic IgG with age, we measured DNA-specific and chromatin-specific IgM and IgG autoantibodies in serum of unchallenged 8–10 months old mice. The autoantibody titers were similar in old wildtype and WASp$^{-/-}$N-WASp$^{fl/fl}$CD19$^{Cre/+}$ mice (Fig. 2C and D), suggesting that the higher titers of IgM autoantibodies in young WASp$^{-/-}$N-WASp$^{fl/fl}$CD19$^{Cre/+}$ mice do not become pathogenic IgG autoantibodies in old mice. In contrast, old WASp$^{-/-}$ mice had increased titers of DNA- and chromatin-specific IgM and IgG autoantibodies (Fig. 2C and D).

3.3. WASp$^{-/-}$ and WASp$^{-/-}$N-WASp$^{fl/fl}$CD19$^{Cre/+}$ mice form large but unpolarized GCs in response to apoptotic cells

We reasoned that elevated IgM autoantibodies in WASp$^{-/-}$N-WASp$^{fl/fl}$CD19$^{Cre/+}$ mice, and to a lesser extent in WASp$^{-/-}$ mice, could be caused by an altered GC response to autoantigens in these mice. To determine the quality of the GC response, we investigated the B cell compartment in the spleen six days after the last injection of apoptotic cells. Wildtype, WASp$^{-/-}$, and WASp$^{-/-}$N-WASp$^{fl/fl}$CD19$^{Cre/+}$ mice had similar number of total B cells and T_{FH} cells (Fig. 3B and C). Moreover, all mice formed GCs in response to apoptotic cells (Fig. 3A and B). GCs can be divided into two compartments; the DZ that consists of highly proliferating CXCR4^{high}CD83^{low} DZ B cells and the LZ that consists of CXCR4^{low}CD83^{high} LZ B cells [3,6,39]. Upon injection with apoptotic cells, wildtype mice had a DZ:LZ B cell ratio of 2:1, indicating that a large fraction of GC B cells resided in the DZ to proliferate and undergo SHM (Fig. 3D). This polarization of GCs was not as evident in WASp$^{-/-}$ or in WASp$^{-/-}$N-WASp$^{fl/fl}$CD19$^{Cre/+}$ mice, where the ratio between LZ and DZ was closer to 1:1 (Fig. 3D). We next examined the polarization of GCs on spleen sections by defining the localization of CD35^{+} FDCs. Wildtype mice showed a distinct separation of the DZ and LZ where CD35^{+} FDCs defined the LZ area and covered 67.2 ± 12.8% of the GC areas closest to the MZ (Fig. 3E). In WASp$^{-/-}$ and WASp$^{-/-}$N-WASp$^{fl/fl}$CD19$^{Cre/+}$ mice, CD35^{+} FDCs covered 85.8 ± 12.8% and 78.7 ± 15.3%, respectively, of the GC area, indicating failure to polarize CD35^{+} FDCs in GCs (Fig. 3E). Moreover, CD35^{+} FDCs covered a large part of the B220^{+} B cell follicles in WASp$^{-/-}$ and WASp$^{-/-}$N-WASp$^{fl/fl}$CD19$^{Cre/+}$ mice (57.3 ± 11.8% and 66.1 ± 7.3%, respectively) as compared to wildtype mice (39.3 ± 4.3% CD35^{+} FDCs of B220^{+} B cell follicles; Fig. 3E). Despite decreased polarization of GCs, wildtype, WASp-/~, and WASp$^{-/-}$N-WASp$^{fl/fl}$CD19$^{Cre/+}$ mice had similar number of total CD138^{+}B220^{-} plasma cells and IgG1^{+} plasma cells (Fig. 3F). Wildtype mice had a large proportion of IgG1^{+} cells in GCs, while WASp$^{-/-}$mice had IgG1^{+} cells both in GCs and extrafollicular foci, and WASp$^{-/-}$N-WASp$^{fl/fl}$CD19$^{Cre/+}$ mice had IgG1^{+} cells exclusively in the red pulp (Fig. 3G). Together, WASp$^{-/-}$ and WASp$^{-/-}$N-WASp$^{fl/fl}$CD19$^{Cre/+}$ mice formed large GCs in response to apoptotic cells, however, their GCs lacked the clear polarization into LZ and DZ zones.

3.4. Increased retention and decreased proliferation of GC B cells in WASp$^{-/-}$ and WASp$^{-/-}$N-WASp$^{fl/fl}$CD19$^{Cre/+}$ mice

Having shown that GCs in WASp$^{-/-}$ and WASp$^{-/-}$N-WASp$^{fl/fl}$CD19$^{Cre/+}$ mice were less polarized, we next examined the cell fate decision for GC B cells to define how long they

stay in the GCs (retention) and how much they proliferate in the GCs. Mice were fed with the DNA incorporating agents EdU and BrdU in the drinking water after the third and fourth injection of apoptotic cells, respectively (Fig. 4A). All cells that proliferated during the third week of the apoptotic cell immunization would incorporate EdU into their DNA and those still present in GCs at day 27 (14 days after the injection) were defined as EdU-retaining cells. Wildtype mice had few EdU-retaining B cells in the GCs at day 27, suggesting that many of the EdU^+ cells after the third immunization with apoptotic cells had diluted the EdU by proliferation and/or already left the GCs to become plasma cells and memory cells (Fig. 4B). Compared to wildtype mice, $WASp^{-/-}$ and $WASp^{-/-}$N-$WASp^{fl/fl}CD19^{Cre/+}$ mice had increased proportion of EdU^+ B cells that were retained in GCs (Fig. 4B). To investigate the proliferation ability of GC B cells we changed EdU to BrdU in the drinking water after the last immunization with apoptotic cells. Wildtype mice had increased proportion of $BrdU^+$ GC B cells as compared to $WASp^{-/-}$ and $WASp^{-/-}$N-$WASp^{fl/fl}CD19^{Cre/+}$ mice (Fig. 4C), supporting the finding that wildtype mice had a large proportion of proliferating $BrdU^+$ cells in the DZ. Together these results suggest that B cells lacking WASp family members were retained longer and proliferated less in GCs.

3.5. $WASp^{-/-}$ and $WASp^{-/-}$N-$WASp^{fl/fl}CD19^{Cre/+}$ B cells can compete for help from wildtype T cells

To determine the competitive fitness of $WASp^{-/-}$ and $WASp^{-/-}$N-$WASp^{fl/fl}CD19^{Cre/+}$ B cells in the context of wildtype T cells we generated mixed BM chimeras. $WASp^{-/-}$ or $WASp^{-/-}$N-$WASp^{fl/fl}CD19^{Cre/+}$ (expressing CD45.2) and wildtype (expressing CD45.1) BM cells were injected into lethally irradiated wildtype mice at a 3:1 ratio (Fig. 5A). $WASp^{-/-}$ B cells, and to a larger extent $WASp^{-/-}$N-$WASp^{fl/fl}CD19^{Cre/+}$ B cells, had decreased capacity to repopulate the splenic B cell compartment, evident in both the follicular and MZ subset of B cells (Fig. 5B). In the GC response to apoptotic cells, $WASp^{-/-}$ B cells competed well with wildtype B cells and reached the 3:1 ratio of injected BM cells (Fig. 5B), indicating that $WASp^{-/-}$ B cells have high capacity to enter the GCs in response to autoantigens. While $WASp^{-/-}$N-$WASp^{fl/fl}CD19^{Cre/+}$ B cells could enter GCs in competition with wildtype B cells, the proportion of $WASp^{-/-}$N-$WASp^{fl/fl}CD19^{Cre/+}$ B cells in GCs was decreased as compared to wildtype B cells (Fig. 5B). We next examined T_{FH} cells and found that more than 50% of T_{FH} cells where of wildtype origin (Fig. 5C). Among the $CD138^+B220^-$ plasma cells, $WASp^{-/-}$ and $WASp^{-/-}$N-$WASp^{fl/fl}CD19^{Cre/+}$ B cells competed well with wildtype B cells and reached the 3:1 ratio of injected cells. In generation of $IgG1^+$ plasma cells, $WASp^{-/-}$ B cells competed well with wildtype B cells, while $WASp^{-/-}$N-$WASp^{fl/fl}CD19^{Cre/+}$ B cells showed a disadvantage (Fig. 5B). To test if $WASp^{-/-}$ and $WASp^{-/-}$N-$WASp^{fl/fl}CD19^{Cre/+}$ B cells could present MHC class II – peptides and activate T cells *in vitro*, we loaded B cells with anti-IgM F(ab′)2 coupled to ovalbumin and examined activation of ovalbumin-specific $CD4^+$ T cells from TCR transgenic OT-II mice. Wildtype, $WASp^{-/-}$, and $WASp^{-/-}$N-$WASp^{fl/fl}CD19^{Cre/+}$ B cells formed immunological synapses with wildtype $CD4^+$ T cells as assessed by polarized F-actin to the synapse interphase (Fig. 5E) and had similar capacity to induce proliferation and IL-2 production by antigen-specific T cells (Fig. 5F). Together, these data suggest that upon immunization with apoptotic cells $WASp^{-/-}$ B cells, and to a lesser extent $WASp^{-/-}$N-$WASp^{fl/fl}CD19^{Cre/+}$ B cells, enter GCs

where they can compete for help from wildtype T cells and form a large pool of plasma cells.

3.6. Altered response to NP-KLH in WASp$^{-/-}$N-WASp$^{fl/fl}$CD19$^{Cre/+}$ mice

We next investigated if the altered GC response in WASp$^{-/-}$ and WASp$^{-/-}$N-WASp$^{fl/fl}$CD19$^{Cre/+}$ mice would influence BCR diversification during affinity maturation. Since apoptotic cells contains a complex set of antigens, we instead used the well-characterized T cell-dependent NP-KLH that induces selection of more than 50% NP-specific B cells that express the V heavy chain (V_H) V_H1–186.2 paired with the V light (V_L) λ chain in wildtype mice [40,41]. We first examined NP-specific antibody titers in serum upon injection with NP-KLH. Wildtype and WASp$^{-/-}$ mice showed increased titers of NP-specific IgM in the primary response and IgG1 antibodies in the secondary response when compared to unimmunized mice (Fig. 6A and B). WASp$^{-/-}$N-WASp$^{fl/fl}$CD19$^{Cre/+}$ mice had high titers of NP-specific IgM already before immunization with NP-KLH and IgM titers remained high during the immunization (Fig. 6A). WASp$^{-/-}$N-WASp$^{fl/fl}$CD19$^{Cre/+}$ mice had high titers of NP-specific IgG1 in the secondary response (Fig. 6B). To examine the affinity of NP-specific antibodies in serum, the antibody binding to BSA covered by 26 NP molecules (low affinity) was compared to that of BSA covered with 4 NP molecules (high affinity). Wildtype and WASp$^{-/-}$ mice showed increased affinity of NP-specific IgM and IgG1 at day 28 in the secondary response as determined by a higher ratio of NP_4/NP_{26} reactivity (Fig. 6C and D). WASp$^{-/-}$N-WASp$^{fl/fl}$CD19$^{Cre/+}$ mice showed almost no increase in NP_4/NP_{26} ratio of NP-specific IgM and IgG1 at day 28 when compared to day 0 (Fig. 6C and D), suggesting that WASpA$^{-/-}$N-WASp$^{fl/fl}$CD19$^{Cre/+}$ B cells undergo affinity maturation at a significantly lower rate when compared to wildtype and WASp$^{-/-}$ B cells.

To further characterize the NP-KLH response in WASp$^{-/-}$ and WASp$^{-/-}$N-WASp$^{fl/fl}$CD19$^{Cre/+}$ mice, we examined the BCR repertoire upon NP-KLH immunization. The repertoire of the three largest V_H families; V_H1, V_H2, and V_H5 families was examined by determining the length of the CDR3 region spanning the V-D-J junction. Wildtype, WASp$^{-/-}$, and WASp$^{-/-}$N-WASp$^{fl/fl}$CD19$^{Cre/+}$ mice showed similar Gaussian distribution of the CDR3 lengths in the V_H1, V_H2, and V_H5 families as determined by the R^2 value and number of peaks in the spectrograms (Supplementary Figure S2A-D). We next examined the usage of V_L chains by investigating $V_L\lambda^+$ B cells, known to pair with the V_H1–186.2 chain in the response to NP-KLH [40,41], Both WASp$^{-/-}$ and WASp$^{-/-}$N-WASp$^{fl/fl}$CD19$^{Cre/+}$ mice had increased number of $V_L\lambda^+$ B cells in the red pulp of the spleen and in GCs, when compared to wildtype mice (Fig. 6E and F). Moreover, WASp$^{-/-}$N-WASp$^{fl/fl}$CD19$^{Cre/+}$ mice had increased percentage of NP-specific $V_L\lambda^+$ GC B cells (Fig. 6G). When comparing the NP_8/NP_{24} ratio of NP-specific $V_L\lambda^+$ GC B cells, wildtype, WAS$^{-/-}$, and WASp$^{-/-}$N-WASp$^{fl/fl}$CD19$^{Cre/+}$ mice had similar ratio (Fig. 6H). This suggests that the increased number of NP-specific $V_L\lambda^+$ GC B cells in WASp$^{-/-}$N-WASp$^{fl/fl}$CD19$^{Cre/+}$ mice was not associated with increased affinity maturation. To assess the outcome of $V_L\lambda^+$ B cells, we next examined $V_L\lambda^+$ clones among plasma cells. Despite increased frequency of $V_L\lambda^+$ plasma cells in WASp$^{-/-}$ and WASp$^{-/-}$N-WASp$^{fl/fl}$CD19$^{Cre/+}$ mice (Fig. 6I), wildtype mice had increased percentage of NP-specific $V_L\lambda^+$ plasma cells and of high affinity when compared to $V_L\lambda^+$ plasma cells in WASp$^{-/-}$ and WASp$^{-/-}$N-WASp$^{fl/fl}$CD19$^{Cre/+}$ mice (Fig.

6J and K). Together, this data shows that WASp$^{-/-}$ and WASp$^{-/-}$N-WASp$^{fl/fl}$CD19$^{Cre/+}$ mice formed NP-specific $V_L\lambda^+$ B cell clones but suggests that these clones had limited affinity maturation.

3.7. Altered B cell affinity maturation in WASp$^{-/-}$N-WASp$^{fl/fl}$CD19$^{Cre/+}$ mice

To investigate affinity maturation, we performed SHM analysis of expressed BCRs from GC-enriched B cells of NP-KLH immunized mice. A 5′ primer specific for V_H1-186.2 and a 3′ primer in either constant heavy chain (C) Cμ or Cγ1 were used to detect mutations in IgM and IgG1, respectively. Using this approach, we could detect a specific high affinity mutation in the complementary determining region (CDR)1 replacing a tryptophan with leucine at position 33 (W33L) [40,41]. Wildtype and WASp$^{-/-}$ B cells had high rate of replacement mutations in both IgM and IgG1 (Fig. 7A and B) and 65–80% of the IgG1 clones expressed the high affinity W33L mutation in CDR1 (Fig. 7B, indicated with pink arrowhead). WASp$^{-/-}$N-WASp$^{fl/fl}$CD19$^{Cre/+}$ B cells showed a lower frequency of replacement mutations in both IgM and IgG1 as compared to wildtype and WASp$^{-/-}$ B cells (Fig. 7A and B). Despite low serum titer of NP-specific IgG1 antibodies of high affinity in WASp$^{-/-}$N-WASp$^{fl/fl}$CD19$^{Cre/+}$ mice (Fig. 6D), the majority (75%) of Cγ1 sequences had the high affinity W33L mutation in CDR1, showing a strong, if not exclusive, selection of W33L-expressing B cells. The remaining Cγ1 sequences in WASp$^{-/-}$N-WASp$^{fl/fl}$CD19$^{Cre/+}$ B cells were in germline configuration.

4. Discussion

This study provides evidence for a critical role of WASp and N-WASp in selection of high affinity B cells in GCs and in maintenance of peripheral tolerance checkpoints to avoid production of autoantibodies. The intracellular signaling axis of GEFs, Rho GTPases, and WASp family members regulates BCR signaling to obtain long-lived protective immunity [8,9]. Here we show that WASp$^{-/-}$ and WASp$^{-/-}$N-WASp$^{fl/fl}$CD19$^{Cre/+}$ mice had decreased polarization of GCs associated with bystander production of autoreactive IgG1 and IgM antibodies, respectively. Our data implies that N-WASp expression alone drives WASp-deficient B cells towards autoreactivity (Fig. 7C).

The MZ of the spleen constitutes an important barrier to clear apoptotic cells from the circulating blood [42,43] and MZ DCs can efficiently phagocytose apoptotic cells [37]. Given the low number of MZ B cells and MZ macrophages in WASp$^{-/-}$ and WASp$^{-/-}$N-WASp$^{fl/fl}$CD19$^{Cre/+}$ mice [14], our data implies that the abundant CD11c$^+$ DCs may take up and transport apoptotic cells to the B cell follicle and initiate a GC reaction. However, WASp$^{-/-}$ and WASp$^{-/-}$N-WASp$^{fl/fl}$CD19$^{Cre/+}$ mice had disturbed GC polarization and WASp$^{-/-}$ and WASp$^{-/-}$N-WASp$^{fl/fl}$CD19$^{Cre/+}$ GC B cells proliferated less and were retained longer in GCs. Intravital microscopy of GCs has revealed that B cells form a highly polarized morphology with a leading filopodia and trailing uropod when moving within GCs [7,44]. While WASp$^{-/-}$ B cells have a moderately decreased spreading response, WASp$^{-/-}$N-WASp$^{fl/fl}$CD19$^{Cre/+}$ B cells have almost abolished capacity to spread and form filopodia extension *in vitro* [14]. Moreover, WASp$^{-/-}$ and WASp$^{-/-}$N-WASp$^{fl/fl}$CD19$^{Cre/+}$ B cells have reduced capacity to migrate to CXCL12 *in vitro* and compete poorly with wildtype B

cells in homing from blood into lymphoid organs *in vivo* (this study) [14]. B cells devoid of the receptor for CXCL12, CXCR4, fail to create LZ and DZ areas in GCs and yet $CXCR4^{-/-}$ B cells acquire the phenotypic characteristics of DZ and LZ cells [6,39]. Since $WASp^{-/-}$ and $WASp^{-/-}$N-$WASp^{fl/fl}CD19^{Cre/+}$ B cells express CXCR4, our data implies that the decreased capacity to migrate towards CXCL12 by DZ B cells is the likely cause for failure to polarize GCs in $WASp^{-/-}$ and $WASp^{-/-}$N-$WASp^{fl/fl}CD19^{Cre/+}$ mice. The study here supports the concept that GCs can form and be productive in the absence of clear spatial polarization of DZ and LZ. However, for high rate of SHM and selection, GC polarization is required [4,39].

BCR activation triggers intracellular signaling pathways to localized polymerization of actin at the immunological synapse interphase. Dock8 is a GEF for Rac1, Rac2, and Cdc42 [45]. Since Cdc42 releases the autoinhibited folding of WASp and N-WASp to allow their activation, it is reasonable to predict that $Dock8^{-/-}$, $WASp^{-/-}$ and $WASp^{-/-}$N-$WASp^{fl/fl}CD19^{Cre/+}$ mice would share similar defects in B cell functionality. In fact, all three mutant strains have severely decreased MZ B cells, reduced capacity to form an immunological synapse, decreased GC formation and reduced production of IgG1 antibodies, and still normal BCR-induced proliferation [14,29,45–47]. There are however some notable differences in the GC response as we show here. While $Dock8^{-/-}$ mice have near normal rate of general SHM, they fail to induce high affinity mutations [45]. In contrast, $WASp^{-/-}$N-$WASp^{fl/fl}CD19^{Cre/+}$ mice had low rate of general SHM, and yet induced high affinity mutations in IgG1. Dock8 may allow for selection of B cells with moderate affinity for antigen due to the action of other GEFs, such as Vav1 and Vav2 [48,49], that may bypass Dock8 deficiency to activate WASp family members. In contrast, B cells devoid of both WASp and N-WASp lower BCR signaling to the extent that B cells require the high affinity mutation (V_H1-186.2-W33L) for selection in response to NP-KLH.

Strikingly, $WASp^{-/-}$ B cells showed an intermediate phenotype between wildtype and $WASp^{-/-}$N-$WASp^{fl/fl}CD19^{Cre/+}$ B cells. Similar to wildtype mice, $WASp^{-/-}$ mice had capacity to induce switched IgG autoantibodies and high affinity IgG1 antibodies in response to NP-KLH. Moreover, $WASp^{-/-}$ B cells competed well with wildtype B cells in the GC reaction of BM chimeric mice. Similar to $WASp^{-/-}$N-$WASp^{fl/fl}CD19^{Cre/+}$ mice, $WASp^{-/-}$ B mice had decreased polarization of GCs, increased retention and decreased proliferation of GC B cells. This implies a unique contribution of N-WASp in rescuing some functionality of B cells devoid of WASp. Together with previous reports [14,46,47,50], this suggests that at instances when the antigen has capacity to be at high avidity due to large size or high dose, $WASp^{-/-}$ mice can respond to antigens with normal GC response and switched IgG antibody production. Based on increased IgG autoantibody titers in naive $WASp^{-/-}$ mice (this study) [19,23,24] and in WAS patients [26], we reason that N-WASp rescues BCR signaling threshold enough to induce Ig class switch recombination from IgM to lgG1 and SHM but too little to maintain peripheral tolerance checkpoints [51]. The data presented here suggests a scenario in which $WASp^{-/-}$N-$WASp^{fl/fl}CD19^{Cre/+}$ B cells have increased threshold for BCR activation (Fig. 7). *First*, $WASp^{-/-}$N-$WASp^{fl/fl}CD19^{Cre/+}$ mice had high titers of serum IgM antibodies with broad reactivity to autoantigens that indicates escape of autoreactive B cells during peripheral tolerance checkpoints. *Second*, $WASp^{-/-}$N-$WASp^{fl/fl}CD19^{Cre/+}$ B cells had normal capacity to receive help from wildtype T_{FH} cells as evident in the analysis

of BM chimeras in which WASp$^{-/-}$N-WASp$^{fl/fl}$CD19$^{Cre/+}$ B cells constituted a large proportion of GC cells and plasma cells as well as in the *in vitro* capacity to induce T cell proliferation. *Third*, in response to NP-KLH, WASp$^{-/-}$N-WASp$^{fl/fl}$CD19$^{Cre/+}$ B cells almost exclusively had either high affinity IgG1 antibodies (V_H1-186.2-W33L) or IgG1 antibodies that remained in germline configuration. WASp$^{-/-}$N-WASp$^{fl/fl}$CD19$^{Cre/+}$ B cells with lower affinity for antigen and as a consequence less triggering of BCR may not be selected, likely due to failure to spatially coordinate the BCR immunological synapse [29] combined with decreased capacity to polarize the GC response.

Supplementary Material

Refer to Web version on PubMed Central for supplementary material.

Acknowledgment

We acknowledge the valuable comments from Eva Severinson (Stockholm University), Lill Mårtensson (Göteborg University), and Michael Carroll (Harvard Medical School). This work was supported by PhD fellowships from Karolinska lnstitutet to C.I.M.D., M.-L.T., E.K.G., a PhD fellowship from Fundação para a Ciêencia e a Tecnologia to M.A.P.B., a Swedish Cancer Society postdoctoral fellowship to M.K., the Queen Silvia foundation, the Erik and Edith Fernström foundation, and the Swedish Society for Medical Research to C.I.M.D., as well as the Swedish Research Council, Swedish Cancer Society, Childhood cancer foundation, the European Commission 7th framework program (Marie Curie #249177), Jeansson Foundation, Clas Groschinsky Foundation, Åke Wiberg Foundation, Bergvall Foundation, Swedish Society of Medicine, and Karolinska lnstitutet including Center for Allergy Research to L.S.W. L.S.W. is a Ragnar Söderberg fellow in Medicine.

Abbreviations:

AID	activation induced deaminase
BCR	B cell receptor
C_H	constant heavy chain
DZ	dark zone
FDCs	follicular dendritic cells
GC	germinal center
GEF	guanine exchange factor
Ig	immunoglobulin
LZ	light zone
MZ	marginal zone
NP-KLH	4-Hydroxy-3-nitrophenylacetyl Keyhole Limpet Hemocyanin
N-WASp	neuronal Wiskott-Aldrich syndrome protein
SHM	somatic hypermutation
T_{FH}	T follicular helper

V_L	variable light chain
V_H	variable heavy chain
WAS	Wiskott-Aldrich syndrome
WASp	WAS protein

References

[1]. Jonjic S, Functional plasticity and robustness are essential characteristics of biological systems: lessons learned from KLRG1-deficient mice, Eur. J. Immunol. 40 (2010) 1241–1243. [PubMed: 20373518]

[2]. Muramatsu M, Kinoshita K, Fagarasan S, Yamada S, Shinkai Y, Honjo T, Class switch recombination and hypermutation require activation-induced cytidine deaminase (AID), a potential RNA editing enzyme, Cell 102 (2000) 553–563. [PubMed: 11007474]

[3]. Victora GD, Schwickert TA, Fooksman DR, Kamphorst AO, Meyer-Hermann M, Dustin ML, et al., Germinal center dynamics revealed by multi-photon microscopy with a photoactivatable fluorescent reporter, Cell 143 (2010) 592–605. [PubMed: 21074050]

[4]. Gitlin AD, Shulman Z, Nussenzweig MC, Clonal selection in the germinal centre by regulated proliferation and hypermutation, Nature 509 (2014) 637–640. [PubMed: 24805232]

[5]. Batista FD, Neuberger MS, Affinity dependence of the B cell response to antigen: a threshold, a ceiling, and the importance of off-rate, Immunity 8 (1998) 751–759. [PubMed: 9655489]

[6]. Allen CD, Ansel KM, Low C, Lesley R, Tamamura H, Fujii N, et al., Germinal center dark and light zone organization is mediated by CXCR4 and CXCR5, Nat. Immunol. 5 (2004) 943–952. [PubMed: 15300245]

[7]. Hauser AE, Junt T, Mempel TR, Sneddon MW, Kleinstein SH, Henrickson SE, et al., Definition of germinal-center B cell migration in vivo reveals predominant intrazonal circulation patterns, Immunity 26 (2007) 655–667. [PubMed: 17509908]

[8]. Yuseff MI, Pierobon P, Reversat A Lennon-Dumenil AM, How B cells capture, process and present antigens: a crucial role for cell polarity, Nat. Rev. Immunol. 13 (2013) 475–486. [PubMed: 23797063]

[9]. Moulding DA, Record J, Malinova D, Thrasher AJ, Actin cytoskeletal defects in immunodeficiency, Immunol. Rev. 256 (2013) 282–299. [PubMed: 24117828]

[10]. Thrasher AJ, Burns SO, WASP: a key immunological multitasker, Nat. Rev. Immunol. 10 (2010) 182–192. [PubMed: 20182458]

[11]. Massaad MJ, Ramesh N, Geha RS, Wiskott-Aldrich syndrome: a comprehensive review, Ann. N. Y. Acad. Sci. 1285 (2013) 26–43. [PubMed: 23527602]

[12]. Miki H, Miura K, Takenawa T, N-WASP, a novel actin-depolymerizing protein, regulates the cortical cytoskeletal rearrangement in a PIP2-dependent manner downstream of tyrosine kinases, EMBO J. 15 (1996) 5326–5335. [PubMed: 8895577]

[13]. Snapper SB, Takeshima F, Anton I, Liu CH, Thomas SM, Nguyen D, et al., N-WASP deficiency reveals distinct pathways for cell surface projections and microbial actin-based motility, Nat. Cell. Biol. 3 (2001) 897–904. [PubMed: 11584271]

[14]. Westerberg LS, Dahlberg C, Baptista M, Moran CJ, Detre C, Keszei M, et al., Wiskott-Aldrich syndrome protein (WASP) and N-WASP are critical for peripheral B-cell development and function, Blood 119 (2012) 3966–3974. [PubMed: 22411869]

[15]. Cotta-de-Almeida V, Westerberg L, Maillard MH, Onaldi D, Wachtel H, Meelu P, et al., Wiskott Aldrich syndrome protein (WASP) and N-WASP are critical for T cell development, Proc. Natl. Acad. Sci. U. S. A. 104 (2007) 15424–15429. [PubMed: 17878299]

[16]. Catucci M, Castiello MC, Pala F, Bosticardo M, Villa A, Autoimmunity in Wiskott-Aldrich syndrome: an unsolved enigma, Front. Immunol 3 (2012) 209. [PubMed: 22826711]

[17]. Sullivan KE, Mullen CA, Blaese RM, Winkelstein JA, A multiinstitutional survey of the Wiskott-Aldrich syndrome, J. Pediatr. 125 (1994) 876–885. [PubMed: 7996359]

[18]. Dupuis-Girod S, Medioni J, Haddad E, Quartier P, Cavazzana-Calvo M, Le Deist F, et al., Autoimmunity in Wiskott-Aldrich syndrome: risk factors, clinical features, and outcome in a single-center cohort of 55 patients, Pediatrics 111 (2003) e622–e627. [PubMed: 12728121]

[19]. Humblet-Baron S, Sather B, Anover S, Becker-Herman S, Kasprowicz DJ, Khim S, et al., Wiskott-Aldrich syndrome protein is required for regulatory T cell homeostasis, J. Clin. Invest 117 (2007) 407–418. [PubMed: 17218989]

[20]. Maillard MH, Cotta-de-Almeida V, Takeshima F, Nguyen DD, Michetti P, Nagler C, et al., The Wiskott-Aldrich syndrome protein is required for the function of CD4(+)CD25(+)Foxp3(+) regulatory T cells, J. Exp. Med. 204 (2007) 381–391. [PubMed: 17296786]

[21]. Marangoni F, Trifari S, Scaramuzza S, Panaroni C, Martino S, Notarangelo LD, et al., WASP regulates suppressor activity of human and murine CD4(+)CD25(+)FOXP3(+) natural regulatory T cells, J. Exp. Med. 204 (2007) 369–380. [PubMed: 17296785]

[22]. Adriani M, Aoki J, Horai R, Thornton AM, Konno A, Kirby M, et al., Impaired in vitro regulatory T cell function associated with Wiskott-Aldrich syndrome, Clin. Immunol. 124 (2007) 41–48. [PubMed: 17512803]

[23]. Becker-Herman S, Meyer-Bahlburg A, Schwartz MA, Jackson SW, Hudkins KL, Liu C, et al., WASp-deficient B cells play a critical, cell-intrinsic role in triggering autoimmunity, J. Exp. Med. 208 (2011) 2033–2042. [PubMed: 21875954]

[24]. Recher M, Burns SO, de la Fuente MA, Volpi S, Dahlberg C, Walter JE, et al., B cell-intrinsic deficiency of the Wiskott-Aldrich syndrome protein (WASp) causes severe abnormalities of the peripheral B-cell compartment in mice, Blood 119 (2012) 2819–2828. [PubMed: 22302739]

[25]. Raulet DH, Vance RE, Self-tolerance of natural killer cells, Nat. Rev. Immunol. 6 (2006) 520–531. [PubMed: 16799471]

[26]. Castiello MC, Bosticardo M, Pala F, Catucci M, Chamberlain N, van Zelm MC, et al., Wiskott-Aldrich syndrome protein deficiency perturbs the homeostasis of B-cell compartment in humans, J. Autoimmun. 50 (2013) 42–50. [PubMed: 24369837]

[27]. O'Connell AE, Volpi S, Dobbs K, Fiorini C, Tsitsikov E, de Boer H, et al., Next generation sequencing reveals skewing of the T and B cell receptor repertoires in patients with wiskott-Aldrich syndrome, Front. Immunol 5 (2014) 340. [PubMed: 25101082]

[28]. Simon KL, Anderson SM, Garabedian EK, Moratto D, Sokolic RA, Candotti F, Molecular and phenotypic abnormalities of B lymphocytes in patients with Wiskott-Aldrich syndrome, J. Allergy Clin. Immunol. 133 (2014) 896 e4–899 e4. [PubMed: 24210885]

[29]. Liu C, Bai X, Wu J, Sharma S, Upadhyaya A, Dahlberg CI, et al., N-wasp is essential for the negative regulation of B cell receptor signaling, PLoS Biol. 11 (2013) e1001704. [PubMed: 24223520]

[30]. Wermeling F, Chen Y, Pikkarainen T, Scheynius A, Winqvist O, Izui S, et al., Class A scavenger receptors regulate tolerance against apoptotic cells, and autoantibodies against these receptors are predictive of systemic lupus, J. Exp. Med. 204 (2007) 2259–2265. [PubMed: 17893199]

[31]. Mohan C, Alas E, Morel L, Yang P, Wakeland EK, Genetic dissection of SLE pathogenesis. Sle1 on murine chromosome 1 leads to a selective loss of tolerance to H2A/H2B/DNA subnucleosomes, J. Clin. Invest 101 (1998) 1362–1372.

[32]. Westerberg L, Larsson M, Hardy SJ, Fernandez C, Thrasher AJ, Severinson E, Wiskott-Aldrich syndrome protein deficiency leads to reduced B-cell adhesion, migration, and homing, and a delayed humoral immune response, Blood 105 (2005) 1144–1152. [PubMed: 15383456]

[33]. Li QZ, Zhou J, Wandstrat AE, Carr-Johnson F, Branch V, Karp DR, et al., Protein array autoantibody profiles for insights into systemic lupus erythematosus and incomplete lupus syndromes, Clin. Exp. Immunol. 147 (2007) 60–70. [PubMed: 17177964]

[34]. Carey JB, Moffatt-Blue CS, Watson LC, Gavin AL, Feeney AJ, Repertoire-based selection into the marginal zone compartment during B cell development, J. Exp. Med. 205 (2008) 2043–2052. [PubMed: 18710933]

[35]. Walter JE, Rucci F, Patrizi L, Recher M, Regenass S, Paganini T, et al., Expansion of immunoglobulin-secreting cells and defects in B cell tolerance in rag-dependent immunodeficiency, J. Exp. Med. 207 (2010) 1541–1554. [PubMed: 20547827]

[36]. Alamyar E, Duroux P, Lefranc MP, Giudicelli V, IMGT((R)) tools for the nucleotide analysis of immunoglobulin (IG) and T cell receptor (TR) V-(D)-J repertoires, polymorphisms, and IG mutations: IMGT/V-QUEST and IMGT/HighV-QUEST for NGS, Methods Mol. Biol. 882 (2012) 569–604. [PubMed: 22665256]

[37]. Iyoda T, Shimoyama S, Liu K, Omatsu Y, Akiyama Y, Maeda Y, et al., The CD8+ dendritic cell subset selectively endocytoses dying cells in culture and in vivo, J. Exp. Med. 195 (2002) 1289–1302. [PubMed: 12021309]

[38]. Mevorach D, Mascarenhas JO, Gershov D, Elkon KB, Complement-dependent clearance of apoptotic cells by human macrophages, J. Exp. Med. 188 (1998) 2313–2320. [PubMed: 9858517]

[39]. Schmidt TH, Bannard O, Gray EE, Cyster JG, CXCR4 promotes B cell egress from Peyer's patches, J. Exp. Med. 210 (2013) 1099–1107. [PubMed: 23669394]

[40]. McHeyzer-Williams MG, Nossal GJ, Lalor PA, Molecular characterization of single memory B cells, Nature 350 (1991) 502–505. [PubMed: 2014051]

[41]. Bothwell AL, Paskind M, Reth M, Imanishi-Kari T, Rajewsky K, Baltimore D, Heavy chain variable region contribution to the NPb family of antibodies: somatic mutation evident in a gamma 2a variable region, Cell 24 (1981) 625–637. [PubMed: 6788376]

[42]. Mebius RE, Kraal G, Structure and function of the spleen, Nat. Rev. Immunol. 5 (2005) 606–616. [PubMed: 16056254]

[43]. Peng Y, Martin DA, Kenkel J, Zhang K, Ogden CA, Elkon KB, Innate and adaptive immune response to apoptotic cells, J. Autoimmun. 29 (2007) 303–309. [PubMed: 17888627]

[44]. Allen CDC, Okada T, Tang HL, Cyster JG, Imaging of germinal center selection events during affinity maturation, Science 315 (2007) 528–531. [PubMed: 17185562]

[45]. Randall KL, Lambe T, Johnson AL, Treanor B, Kucharska E, Domaschenz H, et al., Dock8 mutations cripple B cell immunological synapses, germinal centers and long-lived antibody production, Nat. Immunol. 10 (2009) 1283–1291. [PubMed: 19898472]

[46]. Meyer-Bahlburg A, Becker-Herman S, Humblet-Baron S, Khim S, Weber M, Bouma G, et al., Wiskott-Aldrich syndrome protein deficiency in B cells results in impaired peripheral homeostasis, Blood 112 (2008) 4158–4169. [PubMed: 18687984]

[47]. Westerberg LS, de la Fuente MA, Wermeling F, Ochs HD, Karlsson MC, Snapper SB, et al., WASP confers selective advantage for specific hematopoietic cell populations and serves a unique role in marginal zone B-cell homeostasis and function, Blood 112 (2008) 4139–4147. [PubMed: 18772454]

[48]. Tedford K, Nitschke L Girkontaite I Charlesworth A Chan G Sakk V, et al., Compensation between Vav-1 and Vav-2 in B cell development and antigen receptor signaling, Nat. Immunol. 2 (2001) 548–555. [PubMed: 11376343]

[49]. Doody GM, Bell SE, Vigorito E, Clayton E, McAdam S, Tooze R, et al., Signal transduction through Vav-2 participates in humoral immune responses and B cell maturation, Nat. Immunol. 2 (2001) 542–547. [PubMed: 11376342]

[50]. Bosticardo M, Draghici E, Schena F, Sauer AV, Fontana E, Castiello MC, et al., Lentiviral-mediated gene therapy leads to improvement of B-cell functionality in a murine model of Wiskott-Aldrich syndrome, J. Allergy Clin. Immun 127 (2011), 1376–U109. [PubMed: 21531013]

[51]. Wardemann H, Yurasov S, Schaefer A, Young JW, Meffre E, Nussenzweig MC, Predominant autoantibody production by early human B cell precursors, Science 301 (2003) 1374–1377. [PubMed: 12920303]

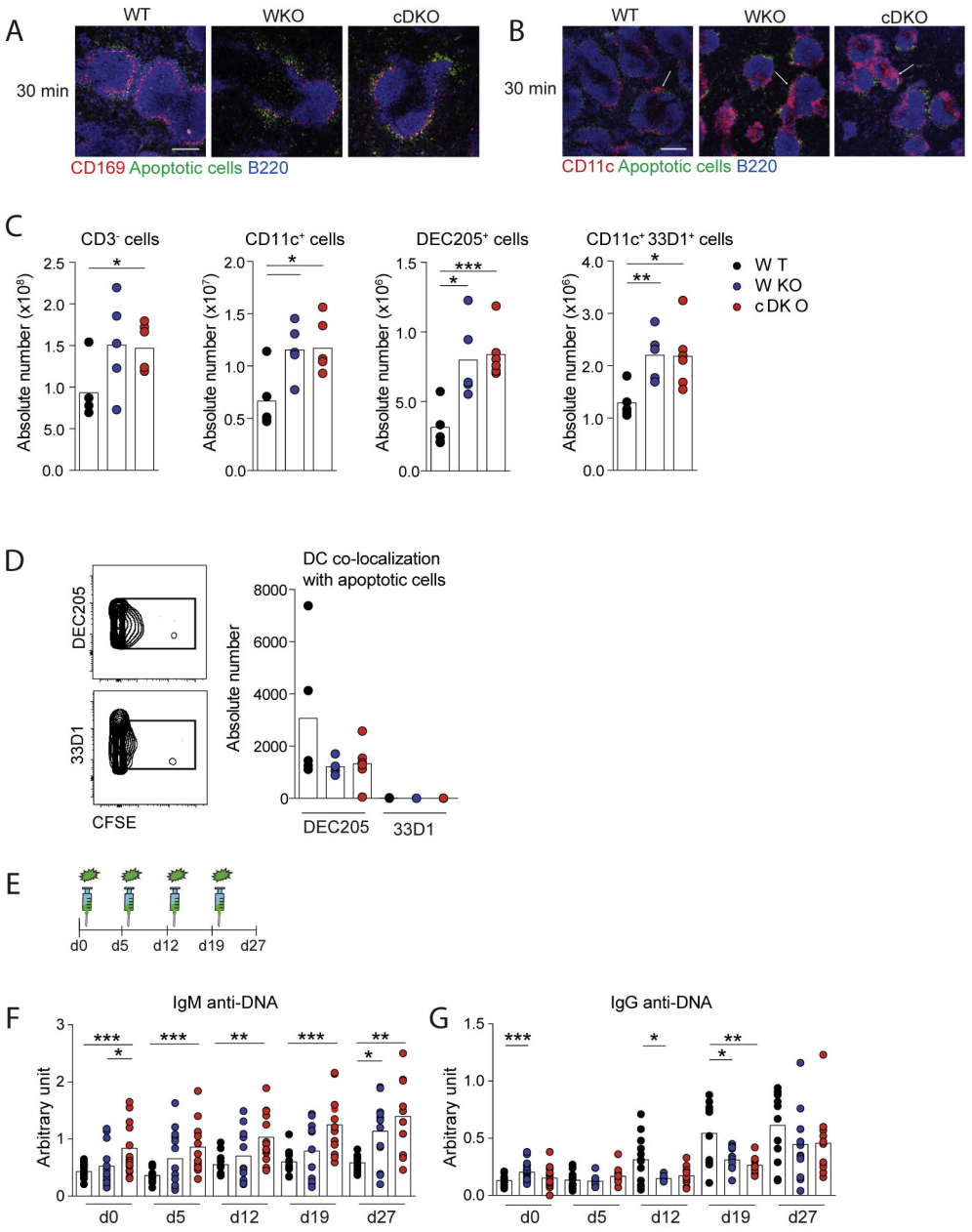

Fig. 1.

$WASp^{-/-}$N-$WASpn^{fl/fl}CD19^{Cre+}$ mice have increased serum titers of DNA-specific IgM antibodies. (A and B) Confocal imaging analysis of spleen sections from mice 30 min after injection with CFSE-labeled apoptotic cells. Representative images of WT and $WASp^{-/-}$ n = 3, $WASp^{-/-}$-N-$WASpn^{fl/fl}nCD19^{Cre+}$ n = 4, are shown. (A) B cells were visualized with B220 (blue), metallophilic macrophages with CD169 (red), and apoptotic CFSE (green). Bars, 150 μm. (B) DCs were visualized with CD11c (red). White arrows indicate co-localization of $CD11c^+$ cells and apoptotic cells. Bars, 300 μm (C and D) Flow cytometry analysis of DC subsets in spleen 30 min after injection with CFSE-labeled apoptotic cells (C) Absolute number of $CD11c^+$ DCs, $CD11c^+DEC2015^+$ DCs, and $CD11c^+33D1^+$ DCs. (D) DC co-localization of CFSE-labeled apoptotic cells shown for $CD11c^+DEC205^+$ and

$CD11c^{+}33D1^{+}$ DCs. WT n = 5, $WASp^{-/-}$ n = 5, $WASp^{-/-}$N-$WASpn^{fl/fl}nCD19^{Cre+}$ n = 6. (E) Mice were injected with apoptotic cells once a week for four weeks. Serum titers of anti-DNA (F) IgM and (G) IgG antibodies were measured at d 0–27. n = 11 –19 and represent a pool of two experiments, each dot correspond to one mouse. Significance was assessed with unpaired, two-tailed Student *t* test. $*P < 0.05$, $**P < 0.01$ and $***P < 0.001$. Data points removed due to lack of sample material: (F) 1 cDKO at d 19, 2 cDKO at d 27 (G) 2 cDKO at d 27. Outliers based on ROUT (Q = 1%) excluded: (F) 1 WKO at d 0, 1 WTat d 27 (G) 1 WKO at d 5, 2 WKO at d 12, 2 WKO at d 19,2 cDKO at d 19. Abbreviations: WKO; $WASp^{-/-}$, cDKO; $WASp^{-/-}$N-$WASp^{fl/fl}CD19^{Cre+}$.

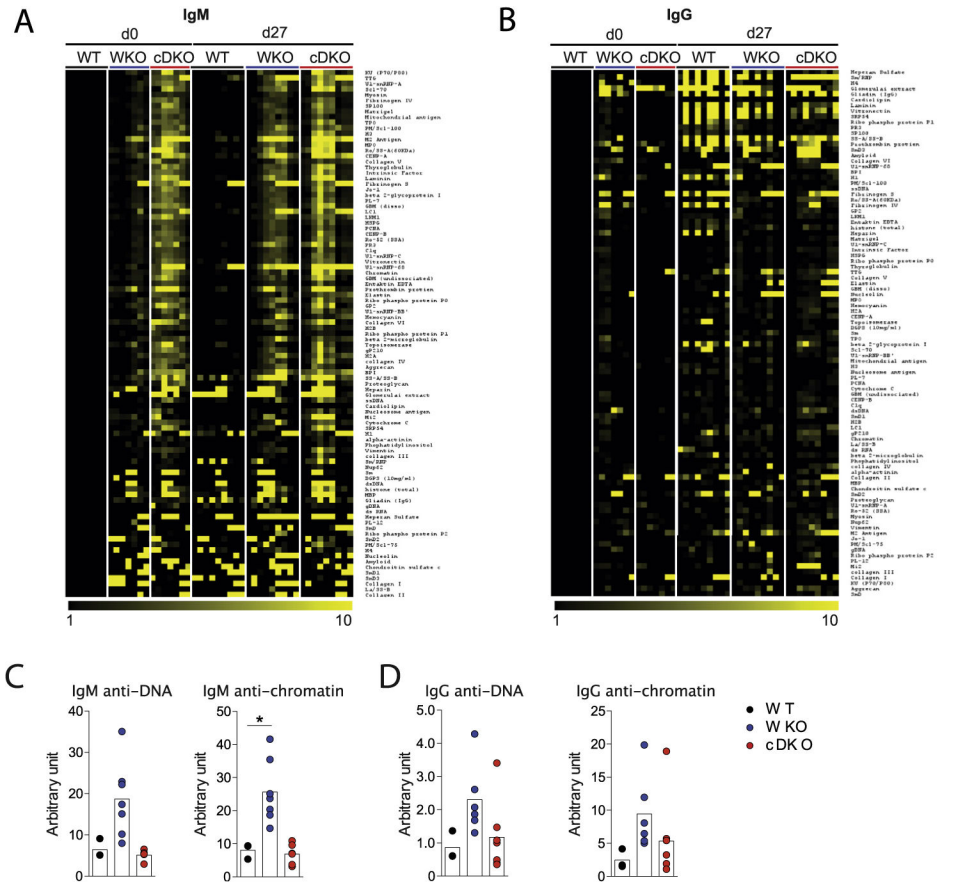

Fig. 2.

Increased autoantibody production in naive WASp$^{-/-}$ and WASp$^{-/-}$N-WASp$^{fl/fl}$CD19^{Cre+} mice. Serum from naïve mice and mice immunized with apoptotic cells were screened for reactivity to 95 different autoantigens using autoantibody array. Autoantigens are sorted by ANOVA starting with lowest p-value at the top for (A) IgM autoantibodies and for (B) IgG autoantibodies. Serum from 7 to 9 mice were tested, data of individual mice are shown. Black color equals ⩽ 1-fold change as compared with average values in control serum (WT d 0). A yellow square indicates a ⩾10-fold increase of autoantibody titer and a black square no difference as compared with average values in control serum. All yellow nuances in between represent a value larger than 1 and smaller than 10. WT, WASp$^{-/-}$, WASp$^{-/-}$N-WASp$^{fl/fl}$CD19$^{Cre/+}$ d 0 n = 7, WT, WASp$^{-/-}$N-WASp$^{fl/fl}$CD19$^{Cre/+}$ d 27 n = 9. (C–D) Autoantibodies in 8–10 weeks old mice. Serum titers of anti-DNA and anti-chromatin (C) IgM and (D) IgG measured in 8–10 weeks old unchallenged mice. WT n = 3, WASp$^{-/-}$ n = 7, WASp$^{-/-}$N-WASp$^{fl/fl}$CD19$^{Cre/+}$ n = 7, each dot correspond to one mouse. Significance was assessed with unpaired, two-tailed Student *t* test. **P* < 0.05. Outliers based on ROUT (Q = 1%) excluded: (C) 2 cDKO anti-DNA, 1 cDKO anti-chromatin (D) 1 WKO anti-DNA, 1 WKO anti-chromatin. Abbreviations: WKO; WASp$^{-/-}$, cDKO; WASp$^{-/-}$N-WASp$^{fl/fl}$CD19$^{Cre/+}$.

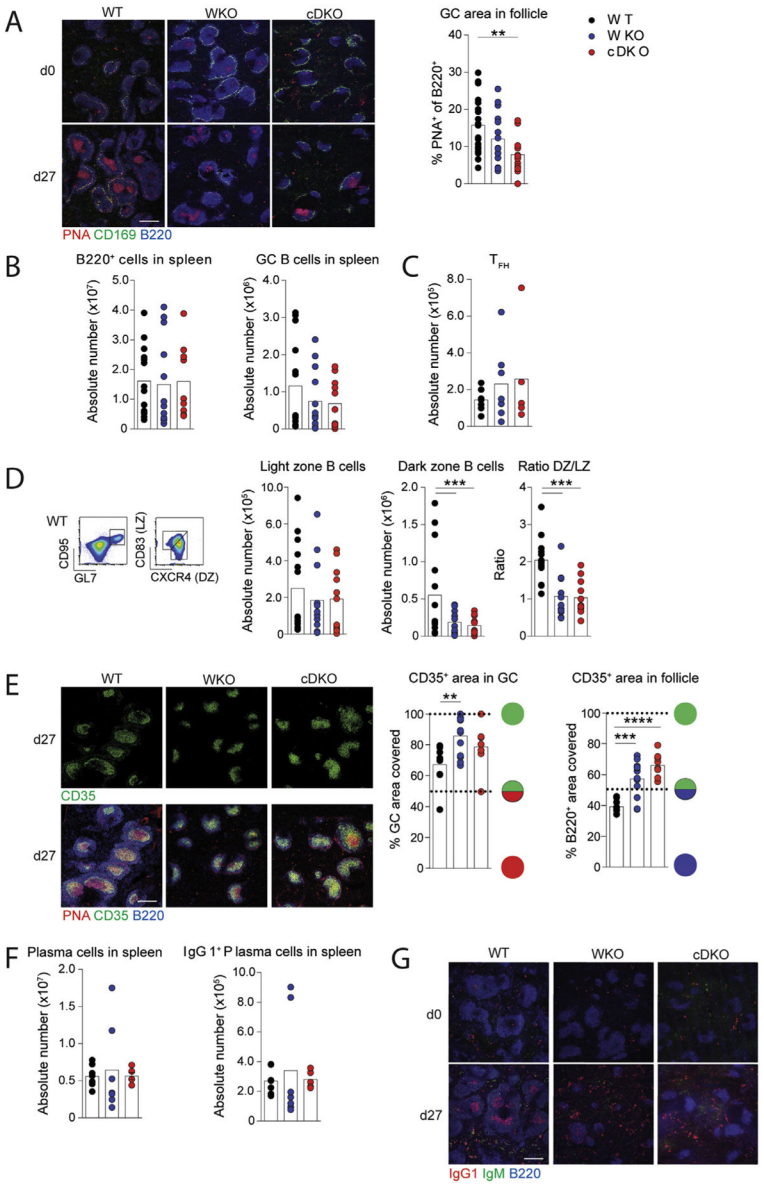

Fig. 3.

Repeated apoptotic cell injections induce a GC response in WT, WASp$^{-/-}$ and WASp$^{-/-}$N-WASp$^{fl/fl}$CD19$^{Cre/+}$ mice. (A) Immunohistochemistry of GC formation in spleen at d 0 and d 27 after apoptotic cell injections. B cells were labeled with B220 (blue), GC cells with PNA (red), and metallophilic macrophages with CD169 (green). Representative pictures from each strain from three experiments are shown. The ratio of GC area of total B220^{+} area in spleen sections is indicated. WT d 0 n = 8, WT d 27 n = 16, WASp$^{-/-}$ d 0 n = 7, WASp$^{-/-}$ d 27 n = 17, WASp$^{-/-}$N-WASp$^{fl/fl}$CD19$^{Cre/+}$ d 0 n = 8, WASp$^{-/-}$N-WASp$^{fl/fl}$CD19$^{Cre/+}$ d 27 n = 16. Bars, 300 μm. (B) Flow cytometry data using B220, GL7 and CD95 to determine quantity of GC B cells. WT n = 14, WASp$^{-/-}$ n = 13, WASp$^{-/-}$N-WASp$^{fl/fl}$CD19$^{Cre/+}$ n = 11. (C) Absolute number of T_{FH} cells (CD4^{+}CD44^{+}CD62L^{-}PD1^{+}CXCR5^{+}) analyzed by flow cytometry. WT n = 8, WASp$^{-/-}$ n = 7, WASp$^{-/-}$N-WASp$^{fl/fl}$CD19$^{Cre/+}$ n = 5. (D) Flow

cytometry data of the GC compartments as determined by LZ B cells ($CD83^{+}CXCR4^{-}$) and DZ B cells ($CD83^{-}CXCR4^{+}$). WT n = 14, $WASp^{-/-}$ n = 13, $WASp^{-/-}$N-$WASp^{fl/fl}CD19^{Cre/+}$ n = 11. (E) Immunohistochemistry for GC polarization. FDCs were labeled with CD35 (green) in spleens at d 27 from mice immunized with apoptotic cells. Upper panel shows CD35 alone and lower panel, CD35 together with PNA (red) and B220 (blue). Representative pictures from each strain from two experiments are shown. The percentage of $CD35^{+}$ area of total PNA^{+} or $B220^{+}$ area in spleen sections is indicated. n = 3 and three images per mouse were analyzed. Bars, 300 μm. (F) Absolute number of total plasma cells ($B220^{-}CD138^{+}$) and $IgG1^{+}$ plasma cells as determined by flow cytometry. WT n = 8, $WASp^{-/-}$ n = 7, $WASp^{-/-}$N-$WASp^{fl/fl}CD19^{Cre/+}$ n = 5. (G) Immunohistochemistry of IgM and IgG1 localization in spleen at d 0 and d 27. WT d 0 n = 3, WT d 27 n = 4, $WASp^{-/-}$ d 0 n = 4, $WASp^{-/-}$ d 27 n = 6, $WASp^{-/-}$N-$WASp^{fl/fl}CD19^{Cre/+}$ d 0 n = 4, $WASp^{-/-}$N-$WASp^{fl/fl}CD19^{Cre/+}$ d 27 n = 6. Bars, 300 μm. Significance was assessed with unpaired, two-tailed Student *t* test. $^{**}P < 0.01$, $^{***}P < 0.001$ and $^{****}P < 0.0001$. Outliers based on ROUT (Q = 1%) excluded: (d) 1 WKO. Abbreviations: WKO; $WASp^{-/-}$, cDKO; $WASp^{-/-}$N-$WASp^{fl/fl}CD19^{Cre/+}$.

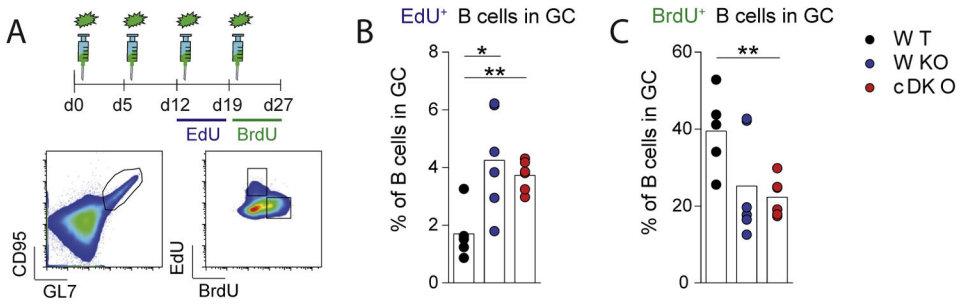

Fig. 4.

Increased retention and decreased proliferation of $WASp^{-/-}$ and $WASp^{-/-}$N-$WASp^{fl/fl}CD19^{Cre/+}$ GC B cells. (A) Proliferating cells were labeled after the third and fourth immunization with apoptotic cells by providing the nucleotide analogous EdU and BrdU in the drinking water for 6 subsequent days. (B and C) Flow cytometry data of (B) EdU^+ or (C) $BrdU^+$ B cells in GCs at d 27. n = 5–6. Note that the gates appear slightly altered because of the staining procedure for EdU and BrdU. Significance was assessed with unpaired, two-tailed Student t test. $*P < 0.05$, $**P < 0.01$. Abbreviations: WKO; $WASp^{-/-}$, cDKO; $WASp^{-/-}$N-$WASp^{fl/fl}CD19^{Cre/+}$.

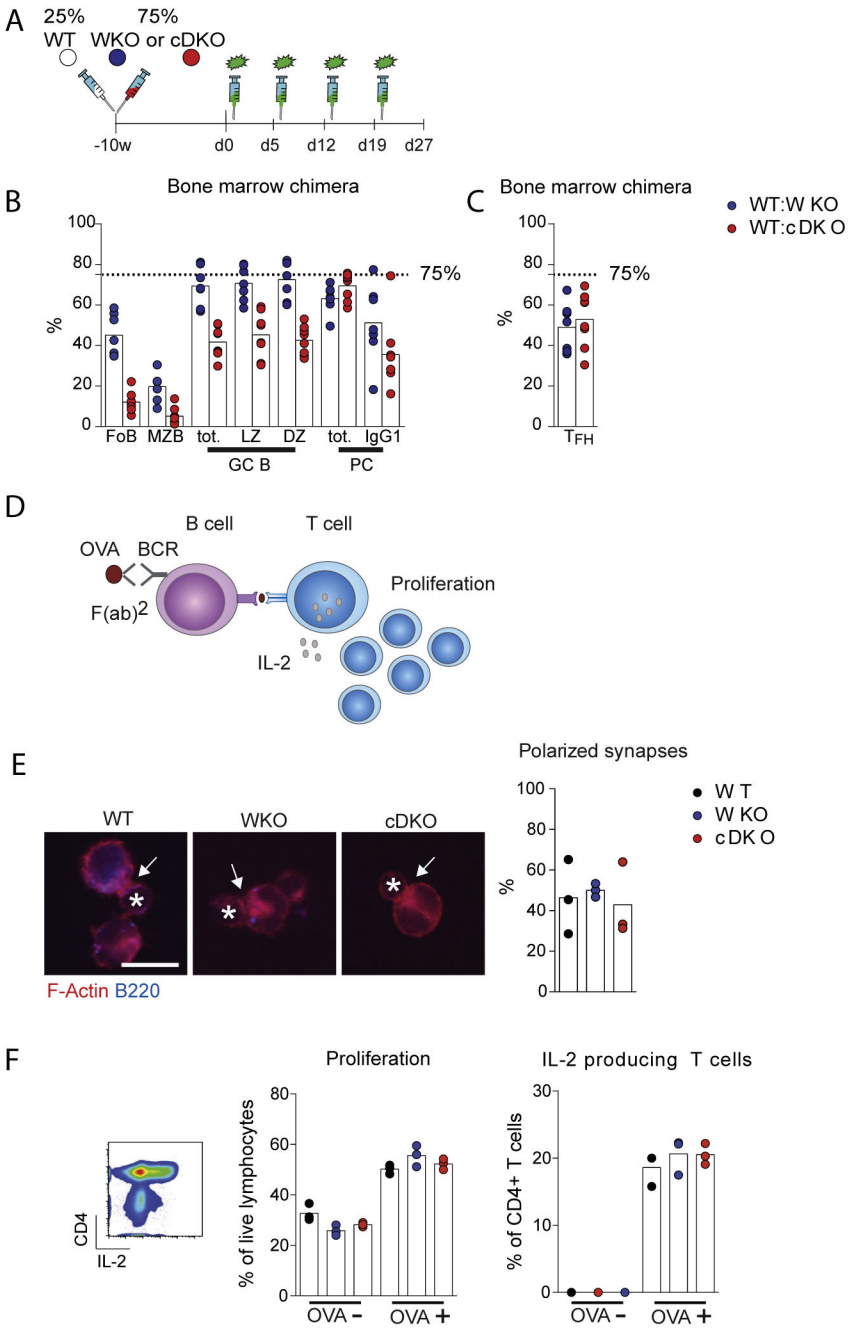

Fig. 5.

WASp$^{-/-}$ and WASp$^{-/-}$N-WASp$^{fl/fl}$CD19$^{Cre/+}$ B cells can compete for help from WT T cells. (A) Generation of BM chimeric mice. WASp$^{-/-}$ or WASp$^{-/-}$-WASp$^{fl/fl}$CD19$^{Cre/+}$ (expressing CD45.2) and WT (CD45.1) BM cells at a 3:1 ratio were intravenous injected into lethally irradiated WT recipient mice. Injections of apoptotic cells started 10 weeks after transplantation. Percentage of cells was analyzed by flow cytometry. (B) Follicular B cells (B220^{+}CD23^{+}IgM^{int}CD21^{int}), MZB cells (B220^{+}CD23^{-}IgM^{high}CD21^{high}), total GC cells (B220^{+}GL7^{+}CD95^{+}), LZ B cells (B220^{+}GL7^{+}CD95^{+}CD83^{+}CXCR4^{low}), DZ B cells (B220^{+}GL7^{+}CD95^{+} CD83^{low}CXCR4^{+}), total plasma cells (B220^{-}CD138^{+}) and switched

plasma cells ($B220^{-}CD138^{+}IgG1^{+}$) were investigated at d 27. n = 7 per condition. (C) T_{FH} cells ($CD4^{+}CD44^{+}CD62L^{-}PD1^{+}CXCR5^{+}$) were analyzed at d 27. n = 7 per condition. (D) B cell induced T cell activation *in vitro*. B cells were loaded with ovalbumin (OVA) and thereafter co-cultured with antigen-specific $CD4^{+}$ T cells from OT-II mice. (E) Synapse formation between OVA-loaded B cells and OT-II $CD4^{+}$ T cells quantified by immunohistochemistry. The star indicates the T cell and the arrow indicates a polarized synapse as determined by polymerized actin (F-actin) at the synapse interphase. Representative pictures from each strain from two experiments are shown. Bar, 10 μm n = 3. (F) Proliferation of and IL-2 production by $CD4^{+}$ T cells from OT-II mice was measured by flow cytometry. n = 3. Graphs show three technical replicas and the experiment has been repeated five times with similar results. Abbreviations: WKO; $WASp^{-/-}$, cDKO; $WASp^{-/-}$-N-$WASp^{fl/fl}CD19^{Cre+}$.

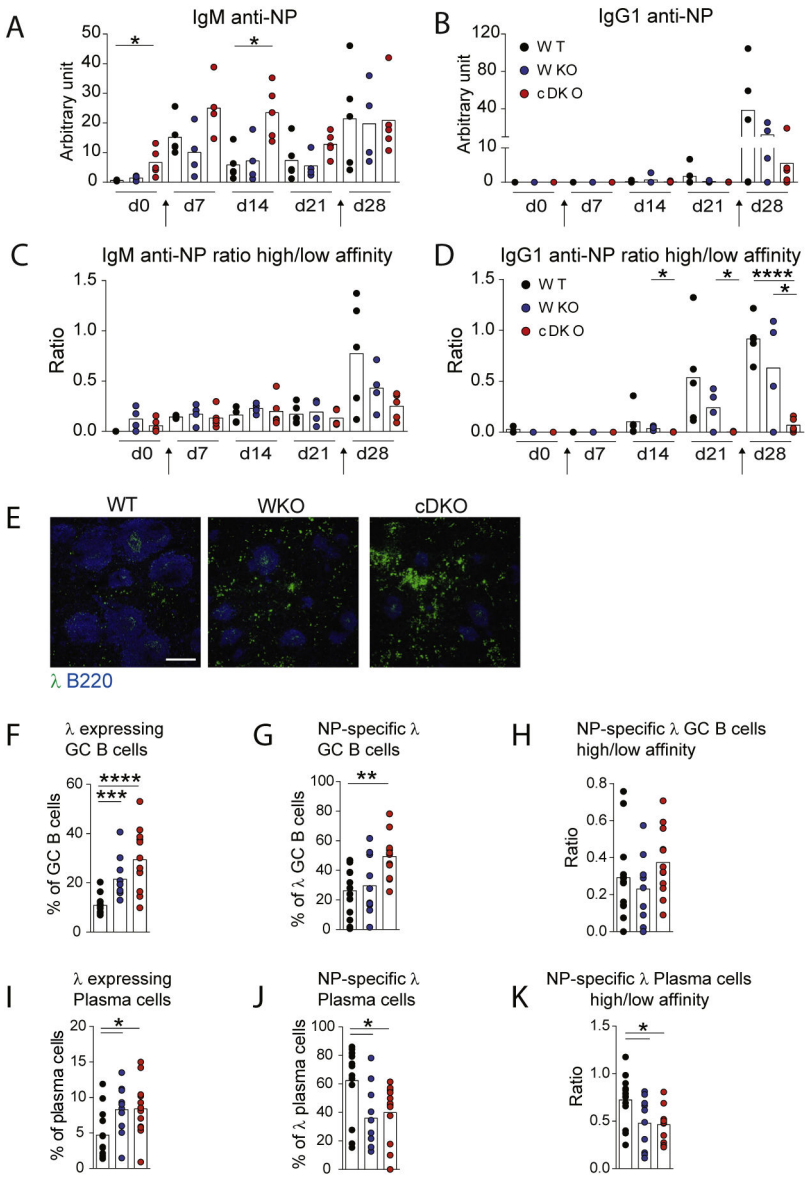

Fig. 6.

Altered response to NP-KLH in WASp$^{-/-}$N-WASp$^{fl/fl}$CD19$^{Cre/+}$ mice. Mice were injected with NP-KLH in alum at d 0, boosted with NP-KLH in PBS at d 21, and analyzed at d 28. (A–D) Serum titers of antibodies reactive to NP were measured once a week during the experiment Arrows indicate time of injections. Total NP-specific (A) IgM and (B) IgGl antibodies as detected using BSA covered by 26 NP molecules. High affinity NP-specific (C) IgM and (D) IgGl antibodies were determined as the capacity to bind to BSA covered by 26 NP molecules (low affinity) to that of BSA covered with 4 NP molecules (high affinity). The NP4/NP26 ratio is indicated as high/low affinity, n = 3–5 and each dot correspond to one mouse. (E) Immunohistochemistry of $V_H\lambda^+$ cells (green) and B cells (blue) in spleen at d 28 upon NP-KLH immunization Bars, 300 pm (F–K) Flow cytometry analysis of NP-specific $V_L\lambda^+$ GC B cells and plasma cells at day 28 upon NP-KLH immunization; (F) $B220^+GL7^+CD95^+V_L\lambda^+$ GC B cells (G), $B220^+GL7^+CD95^+V_L\lambda^+NP24^+$ GC B cells, (H)

ratio of high affinity $B220^{+}GL7^{+}CD95^{+}V_{L}\lambda^{+}NP8^{+}$ and low affinity $B220^{-}GL7^{+}CD95+V_{L}\lambda^{+}NP24^{+}$ GC B cells, (I) $B220^{-}CD138^{+}V^{L}\lambda^{+}$ plasma cells, (J) $B220^{-}CD138^{+}V_{L}\lambda^{+}NP24^{+}$ plasma cells, and (K) ratio of high affinity $B220^{-}CD138+V_{H}\lambda^{+}NP8^{+}$ and low affinity $B220^{-}CD138^{+}V_{H}\lambda^{+}NP24^{+}$ plasma cells. WT n = 13, $WASp^{-/-}$ n = 10, $WASp^{-/-}$N-$WASp^{fl/fl}CD19^{Cre/+}$ n = 12. Significance was assessed with unpaired, two-tailed Student *t* test. $*P < 0.05$, $**P < 0.01$, $***P < 0.001$, and $****P < 0..0001$. Outliers based on ROUT (Q.= 1%) excluded: (C) 1 WT at d 0 (D) 1 WT at d 0, 1 WKO at d 0, 1 WT at d 7, 1 WKO at d 7, 1 cDKO at d 14, 1 cDKO at d 21 (H) 1 WKO. Abbreviations: WKO; WASp”“, cDKO; $WASp^{-/-}$N-$WASp^{fl/fl}CD19^{Cre/+}$.

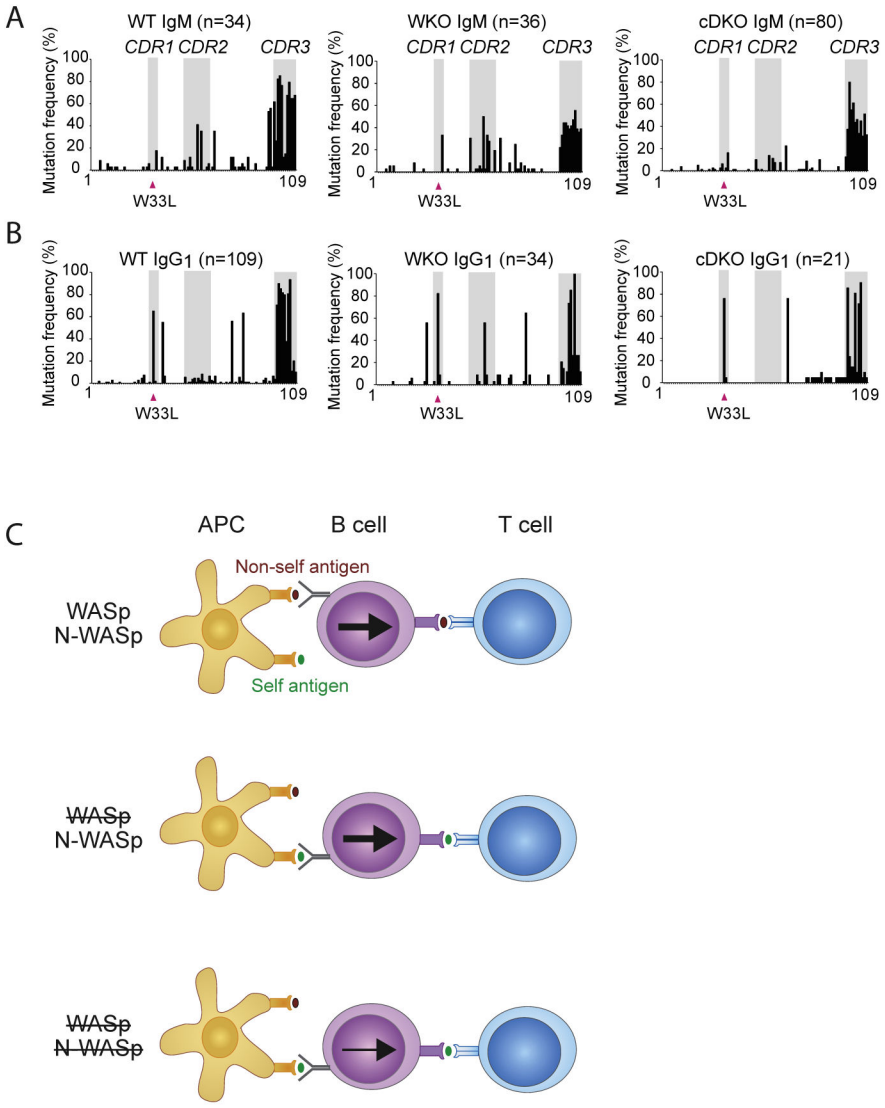

Fig. 7.

Altered B cell affinity maturation in WASp$^{-/-}$N-WASp$^{fl/fl}$CD19$^{Cre/+}$ mice. (A and B) Characterization of replacement mutations found in the V_H1-186.2 family of (A) IgM and (B) IgG1. Grey background highlights the CDR1, CDR2, and CDR3 regions. Pink arrowhead indicates the high affinity amino acid mutation W33L. Amount of unique clones analyzed; WT Cμ n = 34, WT Cγ1 n = 109, WKO Cμ n = 36, WKO Cγ1 n = 34, cDKO Cμ n = 80, cDKO Cγ1 n = 21. (C) Breakdown of peripheral tolerance inWASp deficiency. N-WASp activity in WASp-deficient B cells supports increased reactivity to self antigens. Abbreviations: WKO; WASp$^{-/-}$, cDKO; WASp$^{-/-}$N-WASp$^{fl/fl}$CD19$^{Cre/+}$.